PHYSICAL REVIEW SPECIAL TOPICS - ACCELERATORS AND BEAMS **18,** 040702 (2015)

Model-based optimization of tapered free-electron lasers

Alan Mak,[*] Francesca Curbis, and Sverker Werin
MAX IV Laboratory, Lund University, P.O. Box 118, SE-22100 Lund, Sweden
(Received 18 December 2014; published 23 April 2015)

The energy extraction efficiency is a figure of merit for a free-electron laser (FEL). It can be enhanced by the technique of undulator tapering, which enables the sustained growth of radiation power beyond the initial saturation point. In the development of a single-pass x-ray FEL, it is important to exploit the full potential of this technique and optimize the taper profile $a_w(z)$. Our approach to the optimization is based on the theoretical model by Kroll, Morton, and Rosenbluth, whereby the taper profile $a_w(z)$ is not a predetermined function (such as linear or exponential) but is determined by the physics of a resonant particle. For further enhancement of the energy extraction efficiency, we propose a modification to the model, which involves manipulations of the resonant particle's phase. Using the numerical simulation code GENESIS, we apply our model-based optimization methods to a case of the future FEL at the MAX IV Laboratory (Lund, Sweden), as well as a case of the LCLS-II facility (Stanford, USA).

DOI: 10.1103/PhysRevSTAB.18.040702 PACS numbers: 41.60.Cr, 41.60.Ap

I. INTRODUCTION

In a free-electron laser (FEL), the technique of tapering involves the variation of the undulator parameter along the undulator line, thereby maintaining the resonance condition as the electrons lose energy to the radiation. This can increase the output power and the energy extraction efficiency, as it has been demonstrated experimentally [1,2].

The effectiveness of this technique relies on the proper optimization of the taper profile. One example is the multidimensional scanning method [3]. Another example is the GINGER self-design taper algorithm [4], which is based on the Kroll-Morton-Rosenbluth (KMR) model [5].

In a previous work [6], we briefly presented a method based on a modification to the KMR model, which involves the manipulation of the resonant particle's phase. In this work, we elaborate on this method and examine the underlying physics in greater detail.

The knowledge about taper optimization is important for the MAX IV Laboratory in the development of an x-ray FEL [7], which is part of the laboratory's long-term strategic plan. The plan includes an extension of the MAX IV linear accelerator to 4–6 GeV, to be used as the driver of the FEL.

Using the numerical simulation code GENESIS [8], we study our taper optimization methods on a case of the future MAX IV FEL, where the electron beam energy at the entrance to the FEL is assumed to be 4 GeV.

To test our methods on a different set of parameters, we also apply the methods to a case of the LCLS-II. The case is defined in Jiao *et al.* [3], based on the design parameters at the time of its publication. We then benchmark our results against a taper profile obtained by Jiao *et al.* [3] from the GINGER algorithm [4].

In this work, the numerical simulations are performed in the steady-state mode. This allows us to focus on the effects of manipulating the resonant particle's phase. Our immediate objective is to demonstrate that our modification to the KMR model gives rise to an enhanced energy extraction efficiency. The study of time-dependent effects, such as side-band growth, is left out from the scope of this work and is to be addressed in a forthcoming article.

II. THEORY

A. Tapered FELs

The resonance condition on the central axis of a FEL is given by the equation

$$\lambda = \frac{\lambda_w}{2\gamma^2}(1 + a_w^2), \tag{1}$$

where λ is the optical wavelength, λ_w is the undulator period, and γ is the electron energy normalized to its rest energy $m_e c^2$. The properties of the undulator are characterized by the rms undulator parameter

$$a_w = \frac{K}{\sqrt{2}} \equiv \frac{e\lambda_w B_w}{2\sqrt{2}\pi m_e c^2}, \tag{2}$$

where e is the absolute value of the electron charge and B_w is the undulator field strength.

---

[*] alan.mak@maxlab.lu.se

During the energy extraction, the electrons lose energy to the optical field. For a FEL with constant a_w, the electron energy γ quickly ceases to satisfy the resonance condition and the FEL power saturates. This severely limits the energy extraction efficiency of the FEL.

To overcome this limit, one can *taper* the FEL by varying a_w as a function of the axial position z, so as to maintain the resonance condition continually as the electrons decelerate. This results in the sustained energy transfer from the electrons to the optical field beyond the initial saturation point.

The function $a_w(z)$ is the taper profile. Our aim is to optimize the taper profile, thereby maximizing the energy extraction efficiency of the tapered FEL. Our approach is to develop methods for such optimization, based on a theoretical model. This model-based approach can shed some light on the physics behind the optimization.

The FEL cases considered in this article are single-pass and seeded. Each uses planar undulators with a constant period λ_w.

B. The KMR model

The Kroll-Morton-Rosenbluth model [5] is a theoretical analysis of tapered FELs based on a one-dimensional relativistic Hamiltonian formulation. It is reviewed in Refs. [9–11].

In phase space, each particle has coordinates (ψ, γ), where γ is the energy normalized to the electron rest energy $m_e c^2$ and ψ is the phase relative to the ponderomotive potential. The essence of the KMR model is the consideration of a resonant particle, with phase space coordinates (ψ_R, γ_R) subject to certain constraints. At any z position along the undulator line, the energy of this particle remains at resonance, given by

$$\gamma_R(z) = \sqrt{\frac{\lambda_w}{2\lambda}[1 + a_w^2(z)]}. \tag{3}$$

Meanwhile, the phase of this particle remains constant along the undulator line, so that

$$\psi_R(z) = \psi_R(0) = \text{constant}. \tag{4}$$

The actual value of the constant phase is chosen by the FEL designer.

With the constraints on γ_R and ψ_R, the taper profile $a_w(z)$ is uniquely determined by the equation of motion in the longitudinal direction, namely

$$\frac{d\gamma_R}{dz} = -\frac{e}{\sqrt{2} m_e c^2} \frac{a_w(z) f_B(z) E_0(z)}{\gamma_R(z)} \sin[\psi_R(z)], \tag{5}$$

where E_0 is the optical field amplitude and

$$f_B(z) = J_0\left(\frac{a_w^2(z)}{2 + 2a_w^2(z)}\right) - J_1\left(\frac{a_w^2(z)}{2 + 2a_w^2(z)}\right) \tag{6}$$

is the Bessel factor for planar undulators.

For efficient energy transfer to the optical field, $\gamma_R(z)$ should be a monotonically decreasing function. Otherwise, the resonant particle would absorb energy from the optical field, thus reducing the power of the FEL. In other words, we need

$$\frac{d\gamma_R}{dz} < 0 \quad \text{for all } z. \tag{7}$$

This has two main consequences. According to Eq. (3), this requires $a_w(z)$ to be a monotonically decreasing function as well. According to Eq. (5), this requires $\sin\psi_R > 0$, thus leading to the restriction $0 < \psi_R < \pi$.

C. The ponderomotive bucket

In phase space, the coordinates (ψ_R, γ_R) of the resonant particle defines the stable point in the ponderomotive bucket, which is often known as the centroid. An equation for the separatrices of the bucket is derived in Ref. [5] and can be rewritten as

$$\gamma_\pm(\psi) = \gamma_R \pm \sqrt{\frac{e\lambda_w a_w f_B E_0}{2\sqrt{2}\pi m_e c^2}}[\cos\psi + \cos\psi_R - (\pi - \psi - \psi_R)\sin\psi_R]^{1/2}. \tag{8}$$

As γ_R decreases with z, the ponderomotive bucket moves together towards smaller γ values. This is known as bucket deceleration and is a feature of tapered FELs.

Particles within the bucket are said to be *trapped*. These particles follow stable orbits around the resonant particle and decelerate together with the bucket. As they decelerate, energy is transferred to the optical field. Particles falling out of the bucket are said to be *detrapped*. Once detrapped, a particle quickly moves away from the resonance condition.

It is therefore apparent that the energy extraction in a tapered FEL relies heavily on the trapping of particles in the bucket. Meanwhile, the bucket's capacity to capture particles depends on its size. Following Ref. [5], we analyze the factors that influence the bucket size.

1. Bucket width

We first concern ourselves with the width of the bucket. Let ψ_1 and ψ_2 be the minimum and maximum ψ values for the bucket. The bucket width is then given by the difference $\psi_2 - \psi_1$. The value ψ_2 can be obtained from the simple equation

$$\psi_2 = \pi - \psi_R, \tag{9}$$

while the value ψ_1 can be obtained from the transcendental equation

$$\cos\psi_1 + \cos\psi_R = (\pi - \psi_R - \psi_1)\sin\psi_R. \tag{10}$$

It is apparent that the values ψ_1 and ψ_2, hence the bucket width, are solely determined by the resonant particle's phase ψ_R. Over the range $0 < \psi_R < \pi/2$, the bucket width $\psi_2 - \psi_1$ decreases with ψ_R. At $\psi_R = \pi/2$, we have $\psi_1 = \psi_2 = \pi/2$, meaning that the bucket has zero width.

2. Bucket height

The bucket height is given by

$$\gamma_+(\psi_R) - \gamma_-(\psi_R) \propto \sqrt{a_w f_B E_0}\,\Gamma(\psi_R), \tag{11}$$

where

$$\Gamma(\psi_R) \equiv \sqrt{\cos\psi_R - \left(\frac{\pi}{2} - \psi_R\right)\sin\psi_R}. \tag{12}$$

Unlike the bucket width, the bucket height depends on a_w and E_0 in addition to ψ_R. The ψ_R dependence of the bucket height is governed by the function $\Gamma(\psi_R)$, which decreases with ψ_R for $0 < \psi_R < \pi/2$ and becomes zero when $\psi_R = \pi/2$. $\Gamma(\pi/2 < \psi_R < \pi)$ is purely imaginary.

3. Bucket area

The area of the bucket is a combination of the width and the height. Mathematically, the bucket area can be obtained by the integral

$$A_\Lambda = \int_{\psi_1}^{\psi_2} [\gamma_+(\psi) - \gamma_-(\psi)]d\psi \propto \sqrt{a_w f_B E_0}\,\alpha(\psi_R), \tag{13}$$

where

$$\alpha(\psi_R) \equiv \frac{\sqrt{2}}{8}\int_{\psi_1}^{\psi_2} [\cos\psi + \cos\psi_R - (\pi - \psi - \psi_R)\sin\psi_R]^{1/2} d\psi. \tag{14}$$

It turns out that the bucket area depends on a_w and E_0 in the same way as the bucket height does. The ψ_R dependence of the bucket area is governed by the function $\alpha(\psi_R)$, which decreases with ψ_R for $0 < \psi_R < \pi/2$ and becomes zero when $\psi_R = \pi/2$.

Choosing $\psi_R \geq \pi/2$ will result in the disappearance of the bucket and the total detrapping of particles, thus making the FEL process impossible. This further restricts the choice of ψ_R to the range $0 < \psi_R < \pi/2$. Within this range, a larger ψ_R leads to a smaller bucket area, hence a smaller trapping fraction.

D. Field equations

During the FEL process, the optical field is amplified through its interaction with the electrons. The evolution of the optical field amplitude E_0 and phase ϕ are described by the field equations, of which a derivation is provided in Ref. [9].

In the resonant particle approximation, we assume that only trapped particles participate in the interaction with the optical field and that all trapped particles have the same γ and ψ as the resonant particle. With this approximation, the evolution of E_0 can be written as

$$\frac{dE_0}{dz} = \frac{1}{\sqrt{2}c\epsilon_0} a_w(z) f_B(z) J_\Lambda(z) \frac{\sin[\psi_R(z)]}{\gamma_R(z)}, \tag{15}$$

where ϵ_0 is the permittivity of free space,

$$J_\Lambda(z) = \frac{ecN_\Lambda(z)}{\pi\sigma_{x,y}^2\lambda} \tag{16}$$

is the current density due to the trapped particles, N_Λ is the number of particles trapped, and $\sigma_{x,y}$ is the rms beam radius. Combining the field equation (15) with the equation of motion (5), we have

$$\begin{aligned} \frac{dE_0}{dz} &= \frac{m_e c}{\epsilon_0 e}\frac{1}{E_0(z)} J_\Lambda(z)\left|\frac{d\gamma_R}{dz}\right| \\ &\propto \frac{1}{E_0(z)} N_\Lambda(z)\left|\frac{d\gamma_R}{dz}\right|. \end{aligned} \tag{17}$$

This shows that the growth rate of the optical field is directly proportional to the number of particles trapped N_Λ and the rate of bucket deceleration $|d\gamma_R/dz|$, but is inversely proportional to the field amplitude itself.

Therefore, in the optimization of a tapered FEL, particle trapping is merely one side of the picture. Maximizing the number of particles trapped is not a sufficient condition for maximizing the optical field strength. On the other side of the picture, the bucket also has to decelerate rapidly enough.

However, there is a conflict between rapid bucket deceleration and maintaining a large number of trapped particles. According to Eq. (5), $|d\gamma_R/dz|$ increases with ψ_R for $0 < \psi_R < \pi/2$. But according to Eq. (14), the bucket area decreases with ψ_R for $0 < \psi_R < \pi/2$. When choosing a ψ_R value, increasing the bucket deceleration rate will inevitably decrease the number of trapped particles and vice versa.

The optimization of a tapered FEL requires a good balance between these two conflicting factors. On one hand, we can sacrifice the bucket deceleration rate in exchange of better trapping. On the other hand, we can also sacrifice trapping in exchange of more rapid bucket deceleration.

E. Modification to the KMR model

In the KMR model, the constraint on the phase ψ_R of the resonant particle is somewhat arbitrary [9]. As an attempt to enhance the energy extraction efficiency further, we propose a modification to the KMR model.

Upon the modification, the resonant particle still maintains the resonant energy γ_R throughout the undulator line according to Eq. (3). However, its phase ψ_R is no longer kept constant. Instead, we now formulate ψ_R as a function of z which increases monotonically from zero. While there are many possible choices of such increasing functions, we can adopt the simplest function

$$\psi_R(z) = gz \quad \text{for some constant } g > 0. \tag{18}$$

In other words, ψ_R increases linearly with z at some gradient g, which is chosen by the FEL designer.

For any function $\psi_R(z)$ that increases monotonically from zero, there exists a value $z = L_d$ such that

$$\psi_R(L_d) = \frac{\pi}{2}. \tag{19}$$

This is when the bucket area becomes zero and total detrapping occurs. We therefore refer to L_d as the *detrapping length*. Note that it is possible to have $L_d > L_w$, where L_w is the total length of the undulator line. With this definition of L_d, the proportionality constant g in Eq. (18) can be written as

$$g = \frac{\pi}{2L_d}. \tag{20}$$

With our modification to the KMR model, ψ_R is smaller upstream and larger downstream. For small z, we sacrifice the bucket deceleration rate for particle trapping. For large z, we increase the bucket deceleration rate at the cost of detrapping more particles. We adopt this strategy for two main reasons as follows.

1. Particle trapping consideration

Particle trapping is more important at the beginning of the undulator line. The fraction of particles captured by the bucket at small z sets a limit on the amount of energy that can be extracted subsequently. With a constant ψ_R, the bucket shrinks abruptly from the full width of 2π to a reduced width of $\psi_2 - \psi_1$. This abrupt decrease in bucket width will lead to the sudden detrapping of a large fraction of particles. In contrast, if $\psi_R(z)$ increases smoothly from zero, the bucket will shrink from the full width of 2π in a gradual manner, which is more favorable for the capturing of particles.

2. Bucket deceleration consideration

Beyond the region of initial particle capturing, it is important to fully utilize bucket deceleration for energy extraction. Under the principle of energy conservation, the energy transferred to the optical field equals the total energy loss of all particles

$$W = m_e c^2 \sum_{i=1}^{N} |\gamma_i(L_w) - \gamma_i(0)|, \tag{21}$$

where N is the total number of particles. With a constant ψ_R, the bucket maintains the same width along z and most of the initially captured particles remain trapped. However, our goal here is not to trap all these particles up until the very end of the undulator line, but to make as many particles lose as much energy as possible. With an increasing ψ_R, the bucket will decelerate at an increasing rate, while shrinking in a gradual manner. With a properly chosen g in Eq. (18), the bucket centroid will experience a larger decrease in γ than in the case of a constant ψ_R over the same undulator length L_w, thus bringing trapped particles to lower energies. Even though the shrinking bucket will lead to gradual detrapping of particles along z, the deceleration of each particle up until the point of detrapping will contribute to the sum in Eq. (21). This, together with the more effective capturing of particles at small z, can result in a larger W.

F. Energy extraction efficiency

It is common to define the energy extraction efficiency of a tapered FEL as the product of the particle trapping and bucket deceleration efficiencies [4,11,12]. For instance, the particle trapping efficiency can be formulated as the normalized bucket width $(\psi_2 - \psi_1)/(2\pi)$ and the bucket deceleration efficiency as $\sin\psi_R$ [11].

However, this formulation is not directly applicable to our modified KMR model, in which ψ_R, ψ_1, and ψ_2 are continuously changing. Furthermore, the particle trapping efficiency is not only influenced by the bucket width, but also by the bucket area, which in turn depends on $E_0(z)$ and $a_w(z)$. Similarly, according to Eq. (5), the bucket deceleration rate $|d\gamma_R/dz|$ also depends on $E_0(z)$ and $a_w(z)$. Within a long undulator line, $E_0(z)$ and $a_w(z)$ can vary significantly and this needs to be taken into account.

We therefore propose a generalized formulation of the energy extraction efficiency as follows. At any axial position z along the undulator line, the number of particles trapped in the bucket is $N_\Lambda(z)$. For a small deceleration $d\gamma_R(z)$ of the bucket, the amount of energy lost by the particles is

$$dW(z) = -N_\Lambda(z) m_e c^2 d\gamma_R(z). \tag{22}$$

Integrating both sides over the entire undulator line gives the total amount of energy extracted:

$$W = -m_e c^2 \int_0^{L_w} N_\Lambda(z) \frac{d\gamma_R}{dz} dz. \tag{23}$$

Meanwhile, the initial energy of the electron beam is $W_{\mathrm{beam}} = N\gamma_0 m_e c^2$. The ratio between W and W_{beam} gives the energy extraction efficiency:

$$\eta \equiv \frac{W}{W_{\mathrm{beam}}} = -\frac{1}{\gamma_0}\int_0^{L_w} f_\Lambda(z)\frac{d\gamma_R}{dz}dz. \qquad (24)$$

Here we have defined the trapping fraction $f_\Lambda(z) \equiv N_\Lambda(z)/N$. At this point, we can clearly see the dependence of the energy extraction efficiency on both the trapping fraction and the bucket deceleration rate. But since they are functions of z, they have to be integrated over z for the entire undulator line.

Next, we invoke Eq. (5), followed by Eq. (3), and rewrite the energy extraction efficiency explicitly as

$$\eta = \frac{e}{\sqrt{2}\gamma_0 m_e c^2}\sqrt{\frac{\lambda}{\lambda_w}}\int_0^{L_w}[E_0(z)f_\Lambda(z) \times \frac{a_w(z)f_B(z)}{\sqrt{1+a_w^2(z)}}\sin[\psi_R(z)]dz]. \qquad (25)$$

In the integral, $\psi_R(z)$ is a predefined function, while $E_0(z)$, $f_\Lambda(z)$, and $a_w(z)$ need to be obtained from numerical simulations. This generalized expression for the energy extraction efficiency serves as a figure of merit for a tapered FEL.

III. METHOD

Based on the KMR model and the modified version, we optimize the taper profile $a_w(z)$ using the numerical simulation code GENESIS [8] in the steady-state mode. The principle is to perform iterative simulations along the entire undulator line, from $z = 0$ to $z = L_w$, with some small step size Δz. The required a_w value at every step Δz is computed according to the model.

In order to compute the a_w value, we substitute Eq. (3) into Eq. (5) and eliminate the variable γ_R. This yields

$$\frac{da_w}{dz} = -\frac{\sqrt{2}e}{m_e c^2}\frac{\lambda}{\lambda_w}f_B(z)E_0(z)\sin[\psi_R(z)]. \qquad (26)$$

If the step size Δz is small enough, we can make the approximation $\Delta z \approx dz$ so that

$$a_w(z+\Delta z) = a_w(z) - \frac{\sqrt{2}e}{m_e c^2}\frac{\lambda}{\lambda_w}f_B(z)E_0(z)\sin[\psi_R(z)]\Delta z. \qquad (27)$$

This is the equation used for the iterative simulations. In particular, $\psi_R(z)$ is a predefined function, for which the value at every z position is known. With a constant ψ_R as defined in Eq. (4), we refer to the method as the ordinary KMR method. With $\psi_R(z)$ modified as in Eq. (18), we refer to the method as the modified KMR method.

In order to use Eq. (27), we also need the initial values of the variables. In particular, $a_w(0)$ is chosen to be resonant with the initial beam energy. $E_0(0)$ is the field amplitude of the seed radiation. In the case of self-amplified spontaneous emission (SASE), the effective shot noise amplitude could be used instead. In each step Δz, we obtain the on-axis $E_0(z)$ from the numerical simulation. Equation (27) then enables us to compute the required a_w value at $z + \Delta z$ from the known values of a_w, f_B, ψ_R, and E_0 at z.

IV. RESULTS AND DISCUSSIONS

A. Application to a MAX IV FEL case

We apply the ordinary KMR method and the modified KMR method to a case of the future MAX IV FEL, in which we assume a 4-GeV and 4-kA electron beam. The main parameters are shown in Table I. A sensitivity study of these parameters can be found in Ref. [13].

To study the behavior of the electron beam, optical beam, and taper profile over a long distance, we simulate a continuous undulator line of length $L_w = 200$ m. For the purpose of beam focusing, we superimpose a FODO lattice on the undulator field. The length of the FODO cell is 5 m. Each cell contains two quadrupole magnets of length 10 cm, whose centers are separated by a longitudinal distance of 60 cm. The field strengths of the quadrupole magnets are adjusted to give the desired average beam size.

1. General results

For the ordinary KMR method, simulations reveal that the FEL power is maximized by choosing $\psi_R = 0.26$ rad. The evolution of various parameters along the undulator line are shown in Fig. 1. For the modified KMR method, the corresponding results for three selected g values, namely 3 mrad/m, 5 mrad/m, and 7 mrad/m, are shown in the same figure. These three g-values correspond to detrapping lengths of 600 m, 300 m, and 220 m, respectively.

As seen in Fig. 1(a), the ordinary KMR method features a slow, steady growth of FEL power throughout the undulator line. At $z = 200$ m, the power reaches 1.5 TW. For the

TABLE I. Main parameters of the MAX IV FEL case used in our simulation studies.

Parameter	Symbol	Value
Electron beam energy	W_{beam}	4 GeV
Energy spread	ΔW_{beam}	40 keV
Beam current	I	4 kA
Normalized emittance	$\varepsilon_{x,y}$	0.2 mm mrad
Average beta	$\bar{\beta}_{x,y}$	20 m
Undulator period	λ_w	20 mm
Radiation wavelength	λ	4 Å
Seed radiation power	P_{in}	0.1 MW

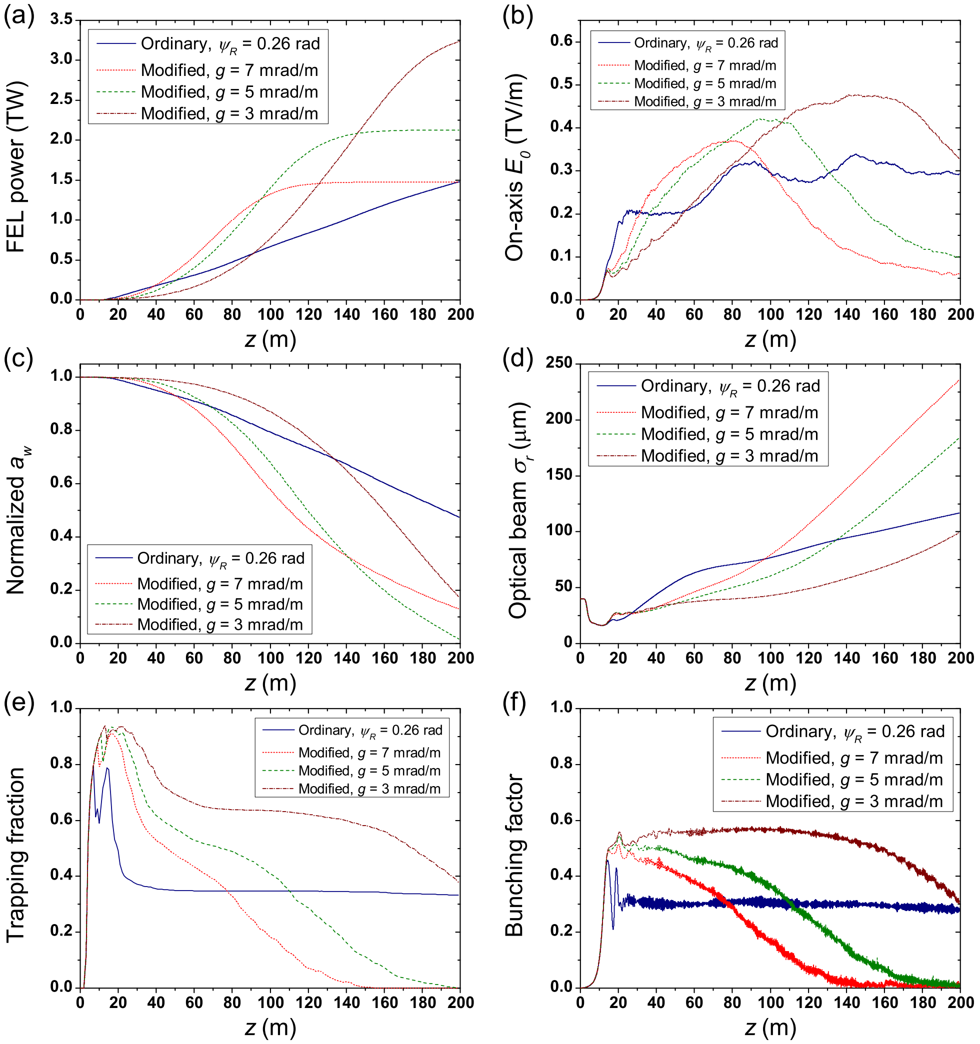

FIG. 1. Evolution of various parameters along the undulator line for the MAX IV FEL case. The parameters are (a) the FEL power, (b) the on-axis optical field amplitude, (c) the a_w parameter normalized to its initial value, (d) the rms radius of the optical beam, (e) the trapping fraction, and (e) the bunching factor. The four curves shown in each plot are the results of the ordinary KMR method with $\psi_R = 0.26$ rad and the modified KMR method with $g = 3$, 5 and 7 mrad/m.

Modified KMR method with $g = 7$ mrad/m, the same final power is attained. However, the power grows much more rapidly and final saturation is reached long before $z = 200$ m. This allows us to obtain the same power while shortening the undulator line to around 130 m, thus reducing the construction cost. With $g = 3$ mrad/m, the power at $z = 200$ m exceeds 3 TW, which is twice that produced by the ordinary KMR method.

In the modified KMR method, a larger g leads to more rapid power growth beyond the initial saturation [see Fig. 1(a)]. However, the final saturation occurs at a lower power and at a smaller z. In contrast, a smaller g leads to slower power growth beyond the initial saturation. However, the final saturation occurs at a higher power and at a larger z. In other words, g can be regarded as an independent adjustment knob for the final saturation power and the final saturation length of a tapered FEL.

The optimal g value depends on the given length of the undulator line. For instance, if the undulator line is shortened to 120 m, it is better to use $g = 5$ mrad/m than to use $g = 3$ or 7 mrad/m, as it yields the highest final power among the three cases. By the same token, if the undulator line is shortened to 80 m, it is better to use $g = 7$ mrad/m.

Figure 1(b) shows the on-axis optical field amplitude E_0 as a function of z. Comparing Figs. 1(a) and 1(b), we see that for the modified KMR method there exists a range of z where E_0 has ceased to grow while the FEL power continues to grow. This is precisely the *radiation power growth region* described in Ref. [3].

Figure 1(c) shows the four resulting taper profiles. The taper profiles resulting from the modified KMR method are more aggressive. The a_w parameter decreases so rapidly that its final value at $z = 200$ m is less than 20% of its initial value.

Figure 1(d) shows the rms radius σ_r of the optical beam as a function of z. For the modified KMR method, there is a correlation between the g value and the optical beam radius. In the deep-tapered region, a smaller g value corresponds to a smaller optical beam radius, which is a manifestation of stronger optical guiding.

There are two types of optical guiding, namely, gain guiding and refractive guiding [10,14]. In a tapered FEL, the latter usually dominates after the initial saturation point [10]. The effects of refractive guiding can be described by a complex-valued refractive index n, as defined in Ref. [14]. The strength of refractive guiding is measured by the real part of n. Under the resonant particle approximation, it can be written as

$$\mathrm{Re}[n(z)] = 1 + \frac{\sqrt{2}\lambda}{4\pi\epsilon_0 c}\frac{a_w(z)f_B(z)J_\Lambda(z)}{\gamma_R(z)E_0(z)}\cos[\psi_R(z)]. \quad (28)$$

With $\psi_R(z)$ as defined in Eq. (18), the strength of refractive guiding varies as $\cos(gz)$. At the same axial position z, a smaller g results in a larger $\cos(gz)$. This partly explains the correlation between the g value and the optical beam radius in Fig. 1(d).

Figure 1(e) shows the trapping fraction f_Λ as a function of z. With the ordinary KMR method, the trapping fraction soon reaches a plateau, meaning that the number of particles in the ponderomotive bucket is almost constant. With the modified KMR method, the trapping fraction is generally higher at small z, which reflects that the initial capturing of particles is more effective. However, the trapping fraction shows a gradual decrease along the undulator line. The larger is g, the faster is the decrease in the trapping fraction. Comparing Figs. 1(a) and 1(e), we see that when the trapping fraction drops to about 0.2, the FEL power begins to saturate.

Figure 1(f) shows the bunching factor as a function of z. Here the bunching factor is defined as

$$b \equiv |\langle e^{-i\psi}\rangle| = \frac{1}{N}\left|\sum_{j=1}^{N} e^{-i\psi_j}\right|. \quad (29)$$

With the resonant particle approximation, the contribution of the detrapped particles to the sum is zero and the sum over the remaining (trapped) particles becomes

$$b = \frac{1}{N}\left|\sum_{j=1}^{N_\Lambda} e^{-i\psi_R}\right| = \frac{N_\Lambda}{N}|e^{-i\psi_R}| = f_\Lambda. \quad (30)$$

In other words, under the resonant particle approximation, the bunching factor equals the trapping fraction. Comparing Figs. 1(e) and 1(f), the bunching fraction is indeed very close to the trapping fraction in the deep-tapered region. This confirms the validity of the resonant particle approximation in the deep-tapered region.

2. Phase space dynamics

Figure 2 shows the phase space snapshots for the two methods at four z positions along the undulator line. For the ordinary KMR method, the width of the ponderomotive bucket is almost the same at all the four z positions [see Fig. 2(a)]. For the modified KMR method, the bucket width decreases along the undulator line [see Fig. 2(b)]. This phenomenon is also reflected by the trapping fraction curve in Fig. 1(e). As the bucket shrinks in width, particles fall out of the bucket, thus leading to a decreasing trapping fraction. With a larger g value, ψ_R increases more rapidly and the bucket shrinks more rapidly, thus causing a faster decrease in trapping fraction.

Figure 3 shows the phase space trajectories of three representative particles in each of the two methods. Each trajectory has the shape of a spiral, which is a result of two combined effects: synchrotron oscillation and bucket deceleration. In synchrotron oscillation, a trapped particle orbits around the centroid of the bucket, whose position is defined by the resonant particle. In bucket

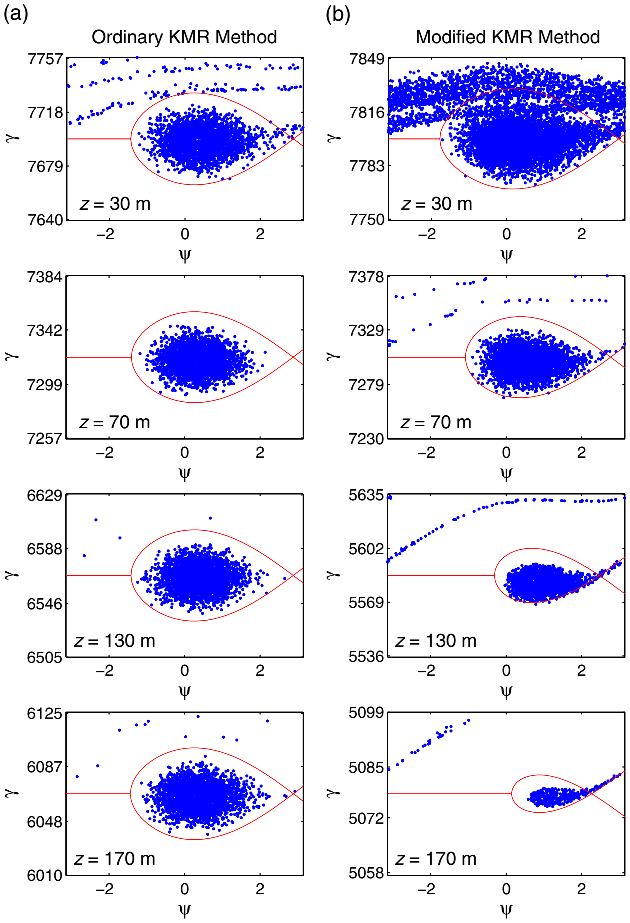

FIG. 2. The (ψ,γ) phase space at four different z positions for the (a) ordinary KMR method (with $\psi_R = 0.26$ rad) and (b) modified KMR method (with $g = 5$ mrad/m). The separatrices of the ponderomotive bucket are shown in red.

deceleration, the bucket centroid itself is moving towards smaller γ.

In the ordinary KMR method, ψ_R remains constant at all z. The trapped particles orbit around a bucket centroid that remains at the same phase [see Fig. 3(a)]. But in the modified KMR method, ψ_R increases with z. The trapped particles orbit around a bucket centroid that moves gradually towards larger phase [see Fig. 3(b)].

The spacing between successive turns in the spiral trajectory is determined by the frequency of the synchrotron oscillations and the rate of the bucket deceleration. The frequency of the synchrotron oscillations is given by [9]

$$\Omega_s(z) = \sqrt{\frac{2\sqrt{2}\pi e}{m_e c^2 \lambda_w} \frac{a_w(z) f_B(z) E_0(z)}{\gamma_R^2(z)} \cos[\psi_R(z)]}, \qquad (31)$$

which varies with ψ_R as $\sqrt{\cos\psi_R}$. The rate of bucket deceleration $|d\gamma_R/dz|$, according to Eq. (5), varies with ψ_R as $\sin\psi_R$. This explains why the increase in the spacing between successive turns is more pronounced in the case of increasing ψ_R [see Fig. 3(b)] than in the case of constant ψ_R [see Fig. 3(a)].

We can also compare the final energy distributions of all particles in the ordinary KMR method and the modified KMR method, as in Fig. 4. The quantity $\gamma(L_w) - \gamma(0)$ is a measure of the energy lost by a particle throughout the undulator line.

For the ordinary KMR method (with $\psi_R = 0.26$ rad), the final energy distribution shows two distinct populations of particles [see Fig. 4(a)]. The particles around $\gamma(L_w) - \gamma(0) = 0$ are those which are not trapped during the initial capturing at small z. The particles around $\gamma(L_w) - \gamma(0) = -2000$ are those which remain trapped in the decelerating bucket up until the end of the undulator line. The former group constitutes about 60% of all particles, while the latter group constitutes about 40%.

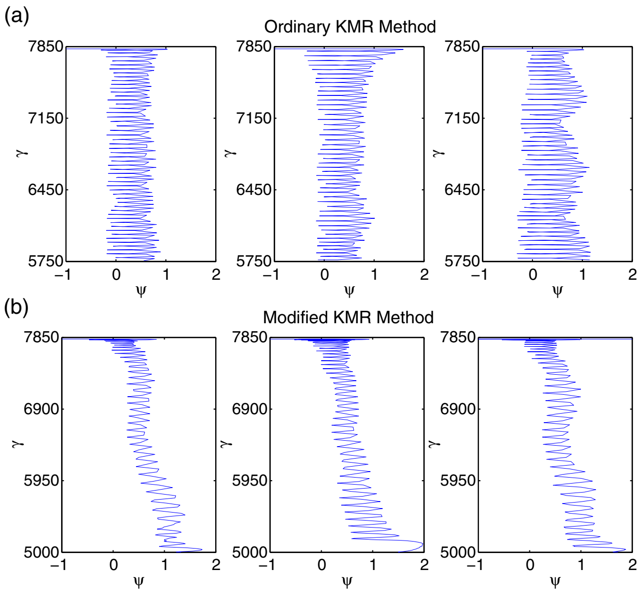

FIG. 3. Particle traces in the (ψ, γ) phase space for the (a) ordinary KMR method (with $\psi_R = 0.26$ rad) and (b) modified KMR method (with $g = 5$ mrad/m). For each of the two methods, the trajectories of three representative, trapped particles are shown.

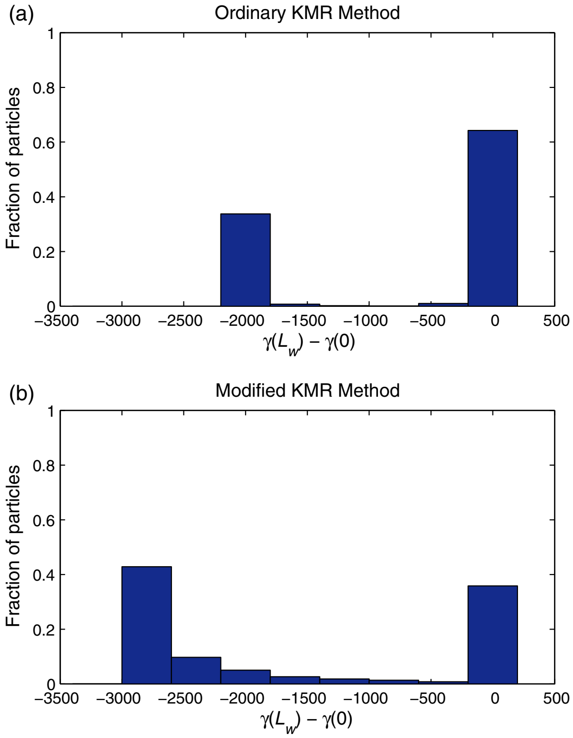

FIG. 4. Histograms showing the particle energy distributions at the end of the undulator line for the (a) ordinary KMR method (with $\psi_R = 0.26$ rad) and (b) modified KMR method (with $g = 3$ mrad/m).

For the modified KMR method (with $g = 3$ mrad/m), the particles around $\gamma(L_w) - \gamma(0) = 0$ constitute only less than 40% of all particles [see Fig. 4(b)], which shows that the initial capturing is more effective than in the ordinary KMR method. The other particles are distributed in a wide range of energies. But comparing the two histograms, the modified KMR method (with $g = 3$ mrad/m) is more effective in bringing more particles to lower energies overall.

In the modified KMR method (with $g = 3$ mrad/m), there is a larger fraction of particles with large $|\gamma(L_w) - \gamma(0)|$ [see Fig. 4(b)]. According to Eq. (21), this results in a larger total energy loss W, hence a larger total energy transfer to the optical field. This also explains the higher final FEL power exhibited in Fig. 1(a).

3. Phase manipulations of different orders

In the modified KMR method, we require $\psi_R(z)$ to be a function that increases monotonically from zero. So far we have adopted the linear function given by Eq. (18), which is the simplest choice. Nonetheless, there are many other possible choices.

As an attempt to find out the optimal choice of $\psi_R(z)$, we explore three additional types of increasing functions, namely, quadratic ($\psi_R \propto z^2$), cubic ($\psi_R \propto z^3$), and square root ($\psi_R \propto z^{1/2}$). For each type of function, we vary the proportionality constant and examine the final FEL power at $z = L_w = 200$ m. The proportionality constant can be expressed in terms of the detrapping length L_d, which is defined in Eq. (19).

Figure 5 shows the variation of the final FEL power with L_d for the four types of functions. In each type of function, there exists an L_d that maximizes the final FEL power. For the linear functions, the maximum attainable final power is 3.2 TW, which occurs at $L_d = 600$ m. For the quadratic functions, the maximum attainable final power is 2.6 TW, which occurs at $L_d = 300$ m. For the cubic functions, the maximum attainable final power is 2.0 TW, which occurs at $L_d = 250$ m. For the square root functions, the maximum attainable final power is 3.0 TW, which occurs at $L_d = 3900$ m.

Comparing the four types of functions in Fig. 5, we see that the higher is the order of $\psi_R(z)$, the smaller is the L_d that maximizes the final power. In terms of maximizing the final FEL power, a linear increase in ψ_R with $L_d = 600$ m is the most favorable choice among all the scenarios studied in Fig. 5.

The optimal order of the increasing function $\psi_R(z)$ can depend on various factors, such as the total length L_w of the undulator line and the electron beam parameters. It can be a parameter for further optimization.

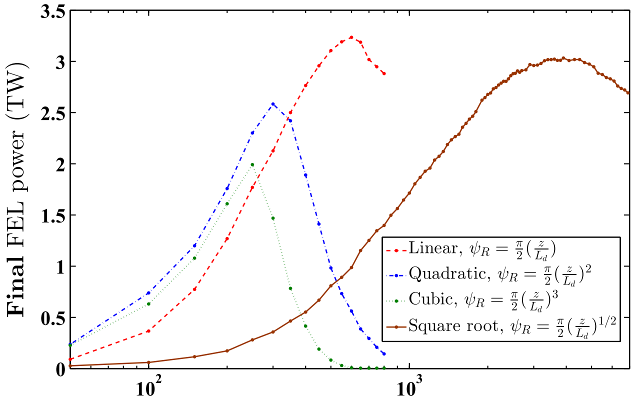

FIG. 5. Comparison of the final FEL powers resulting from different choices of the increasing function $\psi_R(z)$, namely, linear ($\psi_R \propto z$), quadratic ($\psi_R \propto z^2$), cubic ($\psi_R \propto z^3$), and square root ($\psi_R \propto z^{1/2}$). The final FEL power refers to the power at the end of the undulator line ($z = L_w = 200$ m) and is plotted as a function of the detrapping length L_d. Note that the L_d axis is on a logarithmic scale.

4. Energy extraction efficiency

The energy extraction efficiency η, given by Eq. (25), is a figure of merit for a tapered FEL. Using the results of our numerical simulations, we can compute η for the ordinary KMR method and the modified KMR method.

When applying the ordinary KMR method to the MAX IV FEL case, the final power is maximized by choosing $\psi_R = 0.26$ rad. This yields $\eta = 9.3\%$.

When applying the modified KMR method, the final power is maximized by choosing $L_d = 600$ m, which corresponds to $g = 3$ mrad/m. This yields $\eta = 20\%$.

In other words, our modification to the KMR model enables us to obtain more than twice the energy extraction efficiency.

B. Application to an LCLS-II case

We apply the ordinary KMR method and the modified KMR method also to a case of the LCLS-II facility. The case is defined in Jiao *et al.* [3], based on the design parameters at the time of its publication. As before, we simulate a 200-m continuous undulator line. For the ordinary KMR method, simulations reveal that the FEL power is maximized by choosing $\psi_R = 0.2$ rad. For the modified KMR method, the FEL power is maximized by choosing the g value 3 mrad/m.

Jiao *et al.* [3] also shows a taper profile produced by the GINGER self-design taper algorithm [4]. For the purpose of comparison, we extract this taper profile and input it to GENESIS [8] for a steady-state simulation. Since the precise configuration of the strong-focusing lattice is not provided in Jiao *et al.* [3], we have used an *ad hoc* FODO lattice for all the three methods here. The FODO lattice is superimposed on the undulator field and has a cell length of 4.4 m. Each cell contains two quadrupole magnets of length 13 cm, whose centers are separated by a longitudinal distance of 70 cm. The field strengths of the quadrupole magnets are adjusted to achieve the average beam radius of 17.5 μm.

We present the results of these three methods in the same figure. Figure 6(a) shows the evolution of the FEL power along the undulator line. Figure 6(b) shows the corresponding evolution of the optical field amplitude on axis. Figure 6(c) shows the taper profile.

As seen in Fig. 6(a), the final FEL power is 2.7 TW for the ordinary KMR method, 4.1 TW for the GINGER taper profile, and 5.8 TW for the modified KMR method. Out of the three methods, the modified KMR method (with $g = 3$ mrad/m) gives the highest final power.

There is a big difference in final FEL power between the ordinary KMR method and the GINGER algorithm, even though they are both based on the KMR model with constant ψ_R. One explanation for this difference is the treatments of the resonant particle in the two methods.

The ordinary KMR method relies on Eq. (26). When implementing the method, we have always taken $E_0(z)$ to

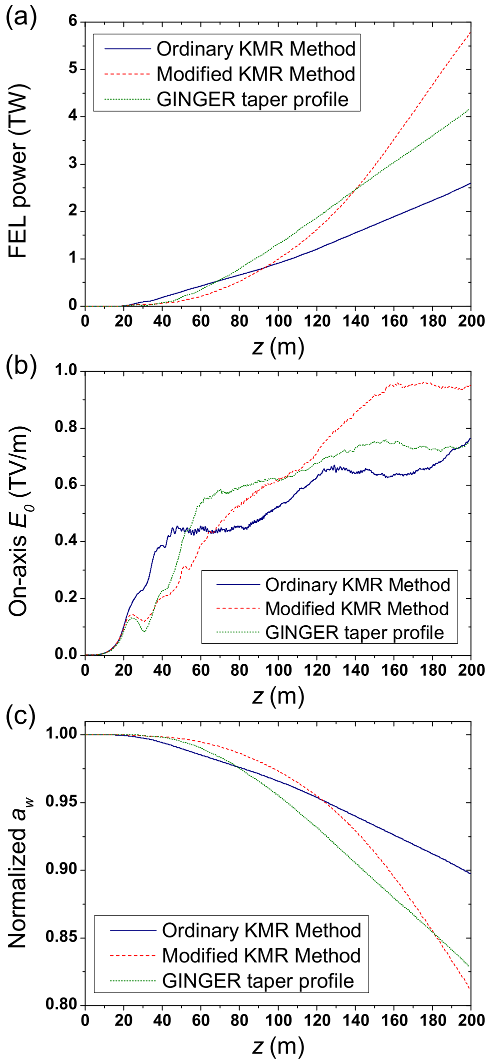

FIG. 6. Evolution of various parameters along the undulator line for the LCLS-II case. The parameters are (a) the FEL power, (b) the on-axis optical field amplitude, and (c) the a_w parameter normalized to its initial value. The three curves shown in each plot are the results of the ordinary KMR method (with $\psi_R = 0.2$ rad), the modified KMR method (with $g = 3$ mrad/m), and the GINGER taper profile from Jiao *et al.* [3].

be the value on the central axis of the FEL. In other words, the resonant particle in our ordinary KMR method is on axis.

But in Jiao *et al.* [3], the resonant particle used for the GINGER algorithm is off axis. It is fixed on the edge of the beam, at a radial position of about 17.5 μm. Using Eq. (26), we can backcalculate the function $\psi_R(z)$ for an on-axis resonant particle from the GINGER-produced taper profile in Fig. 6(c) and the corresponding on-axis $E_0(z)$ in Fig. 6(b). It turns out that $\psi_R(z)$ is not constant, but generally increasing (data not shown), if the resonant particle were to be on axis.

Finally, we compute the energy extraction efficiency η for the three methods according to Eq. (25). In the ordinary KMR method, the final power is maximized by choosing $\psi_R = 0.2$ rad and this yields $\eta = 9.2\%$. In the modified KMR method, the final power is maximized by choosing $g = 3$ mrad/m and this yields $\eta = 26\%$. Meanwhile, the GINGER taper profile gives $\eta = 19\%$. In other words, the modified KMR method gives the highest energy extraction efficiency among the three methods.

C. Undulator segment length

In both the ordinary KMR method and the modified KMR method, the function $a_w(z)$ is determined by iterative numerical simulations. The entire undulator line is divided into segments of length Δz and the required a_w value for each segment is obtained from Eq. (27). In the derivation of Eq. (27), the segment length Δz is assumed to be small. This subsection addresses the requirement on the segment length.

Within each segment Δz, the a_w value is constant. According to Eq. (3), this implies that γ_R is also constant. Recall that γ_R is the γ coordinate of the bucket's centroid in the (ψ, γ) phase space. With a constant γ_R, there is no bucket deceleration.

Meanwhile, the trapped particles continue to undergo synchrotron oscillations. If the segment Δz is long, the trapped particles can make multiple orbits within the nondecelerating bucket. Energy is transferred back and forth between the particles and the optical field. The FEL power then fluctuates, instead of growing steadily, along the undulator line. This can significantly reduce the final power, and hence the energy extraction efficiency, of the FEL.

To avoid this, the bucket must start decelerating again before the trapped particles finish one complete orbit. The distance traveled by a trapped particle down the undulator line during one complete orbit in phase space is the *synchrotron period*, given by

$$T_s(z) = \frac{2\pi}{\Omega_s(z)}. \tag{32}$$

Here Ω_s is the (angular) frequency of synchrotron oscillations given by Eq. (31). Note that T_s has the unit of length and Ω_s has the unit of inverse length. Both T_s and Ω_s are functions of z. Assuming that all the undulator segments have the same length Δz, we need

$$\Delta z < \min[T_s(z)]. \tag{33}$$

For the two FEL cases studied in this article, we have chosen Δz to be 0.5 m. From the simulation results, we compute the function $T_s(z)$ for each case. In the MAX IV FEL case, $\min[T_s(z)]$ ranges from 2.4 to 2.9 m among the four instances presented in Fig. 1. In the LCLS-II case (see Fig. 6), $\min[T_s(z)]$ is 6.0 m for the ordinary KMR method and 5.6 m for the modified KMR method. Thus, the requirement (33) is well satisfied.

V. CONCLUSION

In this work, we have examined the KMR model and proposed a modification to the model. This leads to the ordinary KMR method and the modified KMR method, which are implemented in GENESIS [8] for the purpose of taper optimization. Our modification to the model involves the manipulation of the resonant particle's phase ψ_R. This is motivated by considerations of particle trapping and bucket deceleration. To accommodate our modified KMR model, we have also proposed a generalized formulation for the energy extraction efficiency of tapered FELs.

We have applied the ordinary KMR method and the modified KMR method to two cases, namely, a MAX IV FEL case and an LCLS-II case. In the latter case, a taper profile obtained by Jiao *et al.* [3] from the GINGER self-design taper algorithm [4] is used as a benchmark. In both cases, the modified KMR method yields the highest output power. The results also show that our modification to the KMR model provides a means to enhance the energy extraction efficiency even further.

So far we have compared the different optimization methods by performing numerical simulations in the steady-state mode. Beyond this work, we will continue the studies in the time-dependent mode, so as to provide a better understanding of various time-dependent effects, such as side-band growth. We anticipate to present the results in a forthcoming article.

[1] T. J. Orzechowski *et al.*, High-Efficiency Extraction of Microwave Radiation from a Tapered-Wiggler Free-Electron Laser, Phys. Rev. Lett. **57**, 2172 (1986).

[2] D. F. Ratner *et al.*, in *Proceedings of the 31st International Free-Electron Laser Conference, Liverpool, 2009* (JACoW, Geneva, 2009), pp. 221–224 [http://accelconf.web.cern.ch/AccelConf/FEL2009/papers/tuoa03.pdf].

[3] Y. Jiao *et al.*, Modeling and multidimensional optimization of a tapered free electron laser, Phys. Rev. ST Accel. Beams **15**, 050704 (2012).

[4] W. M. Fawley, Z. Huang, K.-J. Kim, and N. A. Vinokurov, Tapered undulators for SASE FELs, Nucl. Instrum. Methods Phys. Res., Sect. A **483**, 537 (2002).

[5] N. M. Kroll, P. L. Morton, and M. N. Rosenbluth, Free-electron lasers with variable parameter wigglers, IEEE J. Quantum Electron. **17**, 1436 (1981).

[6] A. Mak, F. Curbis, and S. Werin, in *Proceedings of the 5th International Particle Accelerator Conference, Dresden, 2014* (JACoW, Geneva, 2014), pp. 2909–2911 [http://jacow.org/IPAC2014/papers/thpro023.pdf].

[7] S. Werin *et al.*, in *Proceedings of the 36th International Free-Electron Laser Conference, Basel, 2014* (JACoW, Geneva, 2014), pp. 549–552 [http://jacow.org/FEL2014/papers/tup080.pdf].

[8] S. Reiche, GENESIS 1.3: A fully 3D time-dependent FEL simulation code, Nucl. Instrum. Methods Phys. Res., Sect. A **429**, 243 (1999).

[9] D. Prosnitz, A. Szoke, and V. K. Neil, High-gain, free-electron laser amplifiers: Design considerations and simulation, Phys. Rev. A **24**, 1436 (1981).

[10] E. T. Scharlemann, in *High Gain, High Power Free Electron Lasers: Physics and Application to TeV Particle Acceleration*, edited by R. Bonifacio, L. De Salvo Souza, and C. Pellegrini (Elsevier, Amsterdam, 1989), pp. 95–125 [http://www.sciencedirect.com/science/book/9780444873958].

[11] C. A. Brau, in *Free-Electron Lasers* (Academic Press, Boston, 1990), pp. 236–255.

[12] J. M. Slater, Tapered-wiggler free-electron laser optimization, IEEE J. Quantum Electron. **17**, 1476 (1981).

[13] A. Mak, F. Curbis, and S. Werin, in *Proceedings of the 36th International Free-Electron Laser Conference, Basel, 2014* (JACoW, Geneva, 2014), pp. 399–402 [http://jacow.org/FEL2014/papers/tup018.pdf].

[14] E. T. Scharlemann, A. M. Sessler, and J. S. Wurtele, Optical Guiding in a Free-Electron Laser, Phys. Rev. Lett. **54**, 1925 (1985).